

Mpemba Index and Anomalous Relaxation

Israel Klich,¹ Oren Raz,^{2,*} Ori Hirschberg,³ and Marija Vucelja^{1,†}

¹*Department of Physics, University of Virginia, Charlottesville, Virginia 22904, USA*

²*Department of Physics of Complex System, Weizmann Institute of Science, 76100 Rehovot, Israel*

³*Courant Institute of Mathematical Sciences, New York University, New York, New York 10012, USA*

 (Received 18 June 2018; revised manuscript received 6 December 2018; published 26 June 2019)

The Mpemba effect is a counterintuitive relaxation phenomenon, where a system prepared at a hot temperature cools down faster than an identical system initiated at a cold temperature when both are quenched to an even colder bath. Such nonmonotonic relaxations are observed in various systems, including water, magnetic alloys, polymers, and driven granular gases. We analyze the Mpemba effect in Markovian dynamics and discover that a stronger version of the effect often exists for a carefully chosen set of initial temperatures. In this strong Mpemba effect, the relaxation time jumps to a smaller value leading to exponentially faster equilibration dynamics. The number of such special initial temperatures defines the Mpemba index, whose parity is a topological property of the system. To demonstrate these concepts, we first analyze the different types of Mpemba relaxations in the mean-field antiferromagnetic Ising model, which demonstrates a surprisingly rich Mpemba-phase diagram. Moreover, we show that the strong effect survives the thermodynamic limit and that it is tightly connected with thermal overshoot; in the relaxation process, the temperature of the relaxing system can decay nonmonotonically as a function of time. Using the parity of the Mpemba index, we then study the occurrence of the strong Mpemba effect in a large class of thermal quench processes and show that it happens with nonzero probability even in the thermodynamic limit. This study is done by introducing the *isotropic* model for which we obtain analytical lower bound estimates for the probability of the strong Mpemba effects. Consequently, we expect that such exponentially faster relaxations can be observed experimentally in a wide variety of systems.

DOI: [10.1103/PhysRevX.9.021060](https://doi.org/10.1103/PhysRevX.9.021060)

Subject Areas: Soft Matter, Statistical Physics

I. INTRODUCTION

The physics of thermal relaxation is rich with fascinating and often surprising behaviors. A particularly striking and counterintuitive example is provided by the Mpemba effect. Known already to Aristotle [1] but named after a high school student E. B. Mpemba [2], the effect is commonly described as a curious phenomenon where initially prepared hot water freezes faster than cold water under otherwise identical macroscopic conditions when both are cooled by the same cold bath. Because of the complexity of the phenomenon, the precise mechanism and conditions for the occurrence of the Mpemba effect have been under debate. Several explanations have been put forward to the particular mechanism for the Mpemba effect in water. The cause of the Mpemba effect in water has been attributed to evaporation [3], supercooling [4], convection

[5], particular properties of hydrogen bonds [6,7], freezing-point depression by solutes [8], and a difference in the nucleation temperatures of ice nucleation sites between samples [9]. Moreover, the status of the Mpemba effect in water as an experimental finding has been recently called into question [10,11]. Indeed, subtleties of the liquid-solid transition make the precise definition of the effect difficult. For example, when does freezing occur? How well is the freezing point defined? Is a small leftover amount of vapor or liquid tolerated in the description?

It is possible to view the effect as a particular example of a relaxation process far from equilibrium: The Mpemba effect is defined by a quenching process—cooling through a quick change in the ambient temperature achieved by putting the system in contact with a new, colder, thermal bath. In contrast to quasistatic cooling, where the system is in equilibrium at each instant of the cooling process, quenching is, in general, a far-from-equilibrium process. Indeed, anomalous thermal relaxations are not unique to water, and similar effects have been observed in various other systems, e.g., magnetic alloys [12], carbon nanotube resonators [13], granular gases [14], clathrate hydrates [15], polymers [16], and even dilute atomic gas in an optical resonator [17].

Microscopically, the Mpemba effect occurs when the initially hotter system takes a nonequilibrium “shortcut” in

*orenraz@gmail.com

†mvucelja@virginia.edu

Published by the American Physical Society under the terms of the [Creative Commons Attribution 4.0 International license](https://creativecommons.org/licenses/by/4.0/). Further distribution of this work must maintain attribution to the author(s) and the published article's title, journal citation, and DOI.

the system's state space and thus approaches the new equilibrium faster than the initially colder system. A phenomenological description of such a behavior was recently proposed by Lu and Raz within the framework of Markovian dynamics [18]. In this picture, a Mpemba-like behavior can be studied in a large variety of systems (as many processes in physics and chemistry are Markovian [19]), and in particular, in small systems that cannot be adequately described by macroscopic thermodynamics alone. An inverse Mpemba effect (associated with heating processes) can be described similarly. The suggested mechanism for the Mpemba effect raises several natural and important questions: (i) Does the mechanism require fine-tuning of parameters; i.e., does it occur only in singular points of the model's parameter space? Is it robust to small changes in the system parameters? (ii) Does this mechanism survive the thermodynamic limit, or is it only a peculiarity of few-body systems such as those studied in Ref. [18]? One might intuitively expect that this mechanism does not apply to macroscopic systems, since in such systems the probability distribution is highly concentrated on specific points of the system phase space—those that minimize the free energy in equilibrium systems, and hence, even if such shortcuts exist, the system cannot explore them.

The current manuscript contains the following contributions. First, using geometric insights on the relaxation dynamics in probability space, we show that the Mpemba effect may be substantially enhanced on a discrete set of initial temperatures—a phenomenon we call the strong Mpemba effect. We show that these special initial temperatures can be classified by an integer, which we name the Mpemba index, and whose parity is a topological property of the system. Thus, the existence of a strong Mpemba effect is robust to small perturbations in the model parameters. Next, we study the effect in a thermodynamic system focusing on a paradigmatic model: the mean-field Ising antiferromagnet, where a rich Mpemba-phase diagram is found. Using this model, we demonstrate that even though in the thermodynamic limit the probability distribution is concentrated on specific points of phase space, the strong Mpemba effect still exists. Interestingly, we show that the strong Mpemba effect is tightly connected with another type of anomalous thermal relaxation—thermal overshooting—in which the temperature of the system relaxes nonmonotonically in time and overshoots the bath's temperature. We then provide an exact analytical calculation of a strong Mpemba effect probability for an arbitrarily chosen set of energy levels in an idealized “isotropic” model. Comparison of these analytic results with the dynamics of the same set of energy levels with random barriers gives a surprisingly good quantitative agreement. Lastly, we numerically study the strong Mpemba effect in the random energy model (REM) with random barriers and find the scaling of the probability of

the strong effect with the system size. This scaling suggests that again the effect can be observed in the thermodynamic limit.

The manuscript is organized as follows. In Sec. II, we give details on the explicit form of the Markovian dynamics, and in Sec. III, we define the strong Mpemba effect and describe its geometric meaning. Next, in Sec. IV a study of the dynamics of an antiferromagnetic Ising model on a complete bipartite graph reveals a remarkable phase diagram exhibiting a variety of phases with various values of the Mpemba index $\mathcal{I}_M = 0, 1, 2$ and phases with both a direct and inverse strong Mpemba effect. In Sec. IV D, we show that the Mpemba effect also appears in the thermodynamic limit of the antiferromagnetic Ising model, and lastly, in Sec. IV F, we show that in this specific model the strong Mpemba effect implies overshoot in the temperature during relaxation. In Sec. VA, we study the probability of the occurrence of an odd Mpemba index for a system with random barriers taken from a very wide distribution and a fixed set of energies. For this purpose, we use as a model a statistically isotropic ensemble of second eigenvectors of the driving rate matrix. In particular, we find that the probability of a strong Mpemba effect is inversely proportional to the bath temperature, where the proportionality constant depends on the first few moments of the energy level distribution. In Sec. VB, we study the Mpemba effect in the REM with random barriers.

II. SETUP AND DEFINITIONS

We consider Markovian relaxation dynamics, as given by the master equation [20]

$$\partial_t \mathbf{p} = R\mathbf{p}, \quad (1)$$

where $\mathbf{p} = (p_1, p_2, \dots)$, and $p_i(t)$ is the probability to be in state i at time t . Here, the off-diagonal matrix element R_{ij} is the rate (probability per unit time) to jump from state j to i . The state i of the system is associated with an energy E_i , and we focus on relaxation dynamics for which the steady state of Eq. (1) is given by the Boltzmann distribution,

$$\pi_i(T_b) \equiv \frac{e^{-\beta_b E_i}}{Z(T_b)}, \quad (2)$$

where T_b is the temperature of the bath, $Z(T_b) = \sum_i e^{-\beta_b E_i}$ is the partition function at T_b , and throughout the paper $\beta \equiv (k_B T)^{-1}$ is the inverse temperature [in particular, $\beta_b = (k_B T_b)^{-1}$]. Moreover, we also assume that the rate matrix R obeys detailed balance,

$$R_{ij} e^{-\beta_b E_j} = R_{ji} e^{-\beta_b E_i}, \quad (3)$$

and thus can be written in the form (see, e.g., Ref. [21]):

$$R_{ij} = \begin{cases} \Gamma e^{-\beta_b(B_{ij}-E_i)}, & i \neq j, \\ -\sum_{k \neq j} R_{kj}, & i = j, \end{cases} \quad (4)$$

where $B_{ij} = B_{ji}$ can be interpreted as the barrier between the states, and Γ is a constant with the proper units. At long times, the Markov matrix (4) drives an arbitrary initial distribution to the Boltzmann distribution associated with the bath temperature T_b . Note that if the matrix R does not satisfy the detailed balance condition, its steady state does not represent equilibrium since it has nonvanishing current cycles. Interestingly, direct and inverse Mpemba-like effects were recently discovered in driven granular gases where detailed balance is violated [14]. Although our approach may be useful also for such nonequilibrium steady states, for simplicity, we limit our discussion to systems obeying detailed balance.

In the Mpemba effect scenario, the initial condition for Eq. (1) is the thermal equilibrium for some temperature $T \neq T_b$,

$$p_i(T; t=0) = \pi_i(T) \equiv \frac{e^{-\beta E_i}}{Z(T)}. \quad (5)$$

During the relaxation process, the distribution \mathbf{p} , i.e., the solution of Eq. (1), can be written as

$$\mathbf{p}(T; t) = e^{Rt} \boldsymbol{\pi}(T) = \boldsymbol{\pi}(T_b) + \sum_{i>1} a_i(T) e^{\lambda_i t} \mathbf{v}_i, \quad (6)$$

where the rate matrix R has (right) eigenvectors \mathbf{v}_i and eigenvalues λ_i ,

$$R\mathbf{v}_i = \lambda_i \mathbf{v}_i. \quad (7)$$

The largest eigenvalue of R , $\lambda_1 = 0$ is associated with the stationary (equilibrium) distribution $\boldsymbol{\pi}(T_b)$, whereas all the other eigenvalues have a negative real part, $0 > \text{Re}\lambda_2 \geq \text{Re}\lambda_3 \geq \dots$, and they correspond to the relaxation rates of the system. The equilibration timescale is typically characterized by $-(\text{Re}\lambda_2)^{-1}$ [22].

Any detailed balance matrix R can be brought to a symmetric form \tilde{R} via the similarity transformation,

$$\tilde{R} = F^{1/2} R F^{-1/2}, \quad (8)$$

where $F_{ij} \equiv e^{\beta_b E_j} \delta_{ij}$. The matrix \tilde{R} has the same eigenvalues as R , and it has an orthogonal set of real eigenvectors. In particular, $\mathbf{f}_i \equiv F^{1/2} \mathbf{v}_i$ are eigenvectors of \tilde{R} with eigenvalues λ_i . The \mathbf{f}_i -s forms an orthogonal basis, with $\mathbf{f}_i \cdot \mathbf{f}_j = (\mathbf{v}_i \cdot F \mathbf{v}_j) \delta_{ij}$. This form will be useful in what follows.

A. The Mpemba effect

A simple criterion for the presence of a Mpemba effect for the relaxation process in Eq. (1) was given by Lu and Raz [18]. When $|\text{Re}\lambda_2| < |\text{Re}\lambda_3|$ (namely, when they are not equal), the probability distribution (6) can be approximated after a long time as

$$\mathbf{p}(T; t) \approx \boldsymbol{\pi}(T_b) + a_2(T) e^{\lambda_2 t} \mathbf{v}_2. \quad (9)$$

In this case, the Mpemba effect is characterized by the existence of three temperatures: hot, cold, and the bath ($T_h > T_c > T_b$, respectively), such that [23]

$$|a_2(T_h)| < |a_2(T_c)|. \quad (10)$$

The coefficient a_2 can be derived as follows: Multiplying Eq. (6) with $\mathbf{f}_2 F^{1/2}$ from the left, substituting $\mathbf{v}_i = F^{-1/2} \mathbf{f}_i$, and using the fact that \mathbf{f}_i -s forms an orthogonal basis, one gets $\mathbf{f}_2 \cdot F^{1/2} \mathbf{p}(T; t) = a_2(T) \|\mathbf{f}_2\|^2 e^{\lambda_2 t}$. Therefore, for an evolution starting at a given initial probability \mathbf{p}_{init} , we have that a_2 is the corresponding overlap coefficient between the initial probability and the second eigenvector \mathbf{f}_2 :

$$a_2 = \frac{\mathbf{f}_2 \cdot F^{1/2} \mathbf{p}_{\text{init}}}{\|\mathbf{f}_2\|^2}. \quad (11)$$

At the bath temperature, this coefficient vanishes, $a_2(T_b) = 0$ (as in this case $F^{1/2} \mathbf{p}_{\text{init}} = \mathbf{f}_1$, which is orthogonal to \mathbf{f}_2), and it increases in absolute value as the initial temperature departs from the bath. Therefore, to determine whether the Mpemba effect exists, one has to look for nonmonotonicity of $a_2(T)$.

In the next section, we define the strong Mpemba effect, introduce an index to characterize the strong effect, and describe the geometrical interpretation of the effect.

III. THE STRONG MPEMBA EFFECT, ITS INDEX, AND ITS PARITY

Our first contribution is the observation that a stronger effect (even shorter relaxation time) can occur: a process where there exists a temperature $T_M \neq T_b$, such that

$$a_2(T_M) = 0. \quad (12)$$

We call such a situation a strong direct Mpemba effect if $T_M > T_b$ and a strong inverse Mpemba effect if $T_M < T_b$, as at T_M the relaxation process is exponentially faster than for initial temperatures slightly below or above it. Since there is essentially no difference between the direct and inverse effects, we refer to both of them as strong Mpemba effects. The strong Mpemba effect implies the existence of the ‘‘weak’’ effect, as in order to cross zero, a_2 has to be a nonmonotonic function of temperature [because

$a_2(T_b) = 0$, whereas $a_2 \neq 0$ slightly above and below T_b] [24].

To study the strong Mpemba effect, we define the Mpemba indices as

$$\begin{aligned} \mathcal{I}_M^{\text{dir}} &\equiv \# \text{ of zeros of } a_2(T), & T_b < T < \infty, \\ \mathcal{I}_M^{\text{inv}} &\equiv \# \text{ of zeros of } a_2(T), & 0 < T < T_b, \end{aligned} \quad (13)$$

and the total index as

$$\mathcal{I}_M = \mathcal{I}_M^{\text{dir}} + \mathcal{I}_M^{\text{inv}}. \quad (14)$$

$\mathcal{I}_M^{\text{dir}}$ changes its value when the number of zero crossings of the graph of $a_2(T)$ changes in the interval $T_b < T < \infty$. This implies that it is robust, as we discuss in Sec. III A 1.

A. The geometry of the strong Mpemba effect

The geometry of the problem is schematically illustrated in Fig. 1 for a three-state system. The set of all points $\mathbf{p} = (p_1, p_2, p_3)$ which are normalized ($p_1 + p_2 + p_3 = 1$) and non-negative ($p_i \geq 0$) form the probability simplex—the blue triangle in the figure. The set of all Boltzmann distributions $\boldsymbol{\pi}(T)$ form the Boltzmann curve (the red line), which has two boundaries: the $\boldsymbol{\pi}(T = 0)$ where the probability is concentrated at the lowest-energy state (blue point) and $\boldsymbol{\pi}(T = \infty)$, the maximally mixed state in the middle of the simplex where all the states are equally probable (the red point). The set of all \mathbf{p} for which $a_2 = 0$ is illustrated by the intersection of the green plane with the blue triangle. The Boltzmann curve intersects the $a_2 = 0$ plane at $\boldsymbol{\pi}(T_b)$ (pink point) since, being the equilibrium

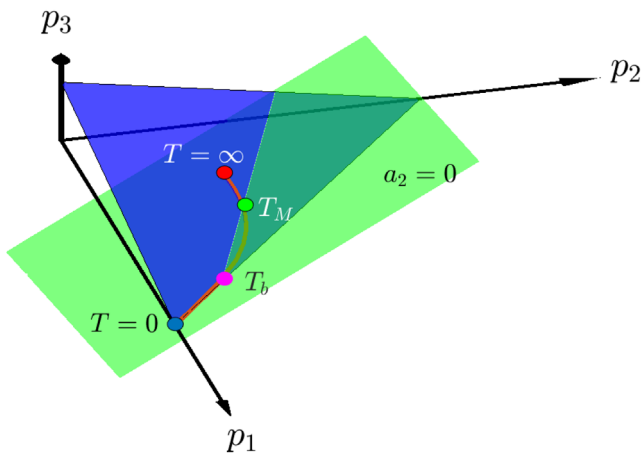


FIG. 1. The geometry of the strong Mpemba effect in a three-state system. The probability simplex is illustrated by the blue triangle. The set of all equilibrium distributions form the red curve. The blue and red points on the curve correspond to $T = 0$ and $T = \infty$. The Mpemba index is nonzero if the equilibrium curve crosses the $a_2 = 0$ plane (green) not only at the bath temperature (illustrated here by the pink point) but also at some other temperature (the green point).

distribution at T_b , $a_2(T_b)$ vanishes by definition. However, in the specific example, the two boundaries of the Boltzmann curve are both on the same side of the $a_2 = 0$ hyperplane; therefore, there must be another point—marked by the green point in the figure—at which the Boltzmann line crosses the $a_2 = 0$ hyperplane again. This point corresponds to T_M where there is a strong Mpemba effect. Topologically, having codimension one, the $a_2 = 0$ hyperplane separates the probability simplex into two disjoint sets. The parity of the number of times a continuous curve crosses this hyperplane depends only on the two boundaries of the curve: If they are both in the same set, then the number of crossings is even, and hence, the parity of \mathcal{I}_M is odd (as it does not count the crossing at T_b), and if they are in a different set, then the number of crossings must be odd, with an even parity for \mathcal{I}_M .

Given T_b , a sufficient condition for the strong direct Mpemba effect to occur is obtained by determining whether a_2 changes sign going from $a_2(T_b + \varepsilon)$ to $a_2(T = \infty)$. This sign change can be expressed by

$$\mathcal{P}(\mathcal{I}_M^{\text{dir}}) \equiv \theta[-\partial_T a_2(T)|_{T=T_b} a_2(T = \infty)], \quad (15)$$

where we use $a_2(T_b + \varepsilon) \approx \partial_T a_2|_{T=T_b} \varepsilon$, and θ is the Heaviside step function. The argument of the step function in Eq. (15) is positive if $a_2(T)$ has an odd number of zero crossings; thus, Eq. (15) describes the *parity* of the number of zeros. In particular, if $\mathcal{P}(\mathcal{I}_M^{\text{dir}}) \neq 0$, we are assured to have at least one crossing, and so $\mathcal{P}(\mathcal{I}_M^{\text{dir}})$ serves as a lower bound on the number of initial temperatures for which the direct strong Mpemba effect occurs. Similarly, the parity for the strong inverse Mpemba effect is

$$\mathcal{P}(\mathcal{I}_M^{\text{inv}}) \equiv \theta[\partial_T a_2(T)|_{T=T_b} a_2(T = 0)], \quad (16)$$

and the parity of the strong Mpemba effect is

$$\mathcal{P}(\mathcal{I}_M) \equiv \theta[a_2(T = \infty)a_2(T = 0)]. \quad (17)$$

As already mentioned above, in some situations there are zeros of $a_2(T)$ that are not accompanied with a sign change. This happens when $a_2(T_M) = 0$ and $a_2'(T_M) = 0$ simultaneously. Such points appear on the boundary between the areas in parameter space with $\mathcal{I}_M = 0$ and $\mathcal{I}_M = 2$, e.g., on the line separating the purple and green areas in Fig. 2. In these cases, $\mathcal{P}(\mathcal{I}_M)$ is no longer the exact parity but still serves as a lower bound to the number of crossings.

Figure 1 provides a helpful three-dimensional picture for the strong Mpemba effect in a three-state system. In fact, the existence of the strong Mpemba effect is always essentially a three-dimensional problem when projected to the proper subplane. As we discuss above, the strong effect can be deduced from the relative directions of the following three vectors: (i) the tangent to the equilibrium line at the bath temperature, (ii) the vector connecting

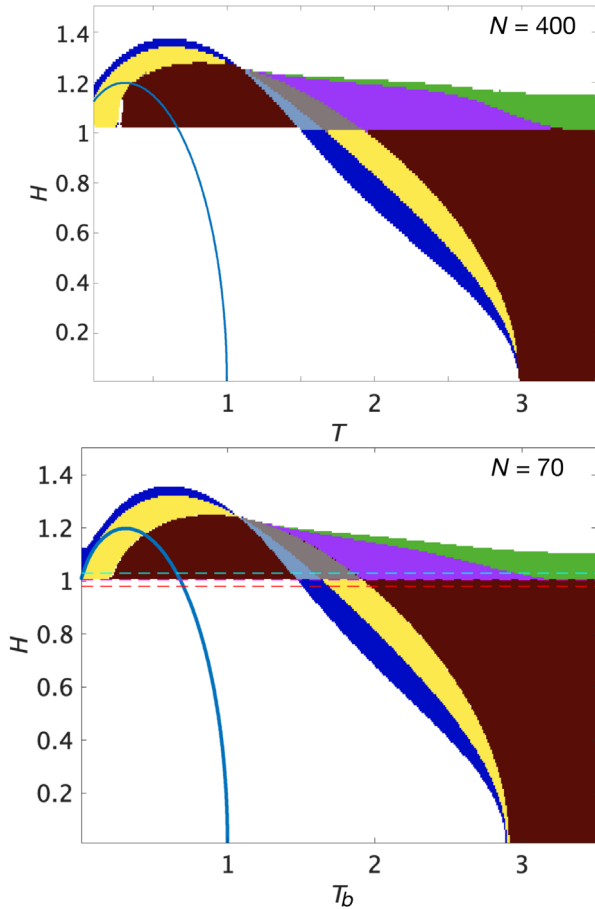


FIG. 2. The mean-field antiferromagnetic Ising model Mpemba-phase diagram. Upper panel: The phase diagram calculated for $N = 400$ spins. There are eight different Mpemba phases in this system: (i) white; no direct or inverse Mpemba effects, (ii) blue; weak direct and no inverse effects, (iii) green; weak inverse and no direct effects, (iv) burgundy; strong inverse with $\mathcal{I}_M^{\text{inv}} = 1$ and no direct effects, (v) violet; strong inverse with $\mathcal{I}_M^{\text{inv}} = 2$ and no direct effects, (vi) light blue; strong inverse with $\mathcal{I}_M^{\text{inv}} = 1$ and weak direct effects, (vii) gray; strong direct with $\mathcal{I}_M^{\text{dir}} = 1$ and strong inverse with $\mathcal{I}_M^{\text{inv}} = 1$, and (viii) yellow; strong direct with $\mathcal{I}_M^{\text{dir}} = 1$ and weak inverse effects. The blue line is the antiferromagnetic-to-paramagnetic phase-transition line of this model calculated in Ref. [25]. Lower panel: The same calculation for $N = 70$ spins. Although the exact location of the boundaries between the different phases is not identical in the two computations, the overall structure is the same. The three dashed lines are lines of constant magnetic field $H = 1.03$, $H = 1$, and $H = 0.97$, and their corresponding equilibrium loci in the thermodynamic limit are given in Fig. 3. Note that the phase diagram has an abrupt jump at $H = 1$, which corresponds to the jump in the equilibrium locus in Fig. 3.

$\pi(T_b)$ and $\pi(T = \infty)$ [or $\pi(T = 0)$ for the inverse effect]), and (iii) the direction of the slowest dynamic v_2 defined in Eq. (7). This observation plays a crucial role in Sec. VA, where we estimate the probability to observe the strong Mpemba effect in a class of random models.

B. Robustness of the Mpemba index

The above geometric interpretation implies that the Mpemba index is a robust quantity, as we discuss next. Consider a small perturbation of order ϵ in the physical quantities, i.e., in the energies, the barriers, and the temperature of the bath. The corresponding change in R is also of order ϵ . This perturbation in R changes both $p_{\text{init}}(T)$ and f_2 , and hence, by Eq. (11), also the graph of $a_2(T)$ in the relevant interval of T . But it does not change $\pi(T = \infty)$, which is always the maximally symmetric point. Similarly, $\pi(T = 0)$ is the lowest-energy point, which changes only if the perturbation changes the ground state by an energy level crossing.

For the perturbation in the physical parameters to change the number of zero crossings, one of the following cases has to occur: (i) p_{init} can change abruptly even with a small perturbation in R if there is a first-order phase transition in the system, and therefore, the equilibrium distribution changes discontinuously. An example for such a case is discussed in Sec. IV D. Note that for this discontinuous change of the equilibrium distribution to happen, the perturbation in the relevant parameters has to be large enough compared to the distance from the value at which there is a first-order phase transition. (ii) f_2 can change abruptly when the perturbation changes the order of λ_2 and λ_3 ; namely, the order of the eigenvalues changes, and therefore, the direction of the eigenvector jumps. As the perturbations of the eigenvalues are of order ϵ too, the spectral gap $\lambda_2 - \lambda_3$ defines the stability region in which these changes are not expected. In other words, if the perturbation in R is small compared to $\lambda_2 - \lambda_3$ then such a jump is not expected. (iii) A small perturbation in R can cause two zeros to “annihilate” each other in a saddle-node bifurcation, and similarly, two new zeros can be generated. However, in these cases, the parity of \mathcal{I}_M does not change. (iv) A zero can move through T_b (this is analogous to a transcritical bifurcation). In such a case, both $\mathcal{I}_M^{\text{dir}}$ and $\mathcal{I}_M^{\text{inv}}$ change by 1, but the parity of \mathcal{I}_M does not change. (v) Lastly, a zero can “vanish” in the $T \rightarrow \infty$ limit or at $T = 0$. But as we discuss above, the end points $\pi(T = 0)$ and $\pi(T = \infty)$ do not move, so a zero can “vanish” only if f_2 changes its direction.

From the five cases discussed above, we can conclude that the parity of \mathcal{I}_M can change only if there is a phase transition in the system, λ_3 becomes larger than λ_2 , or if the perturbation changes the sign of one of $a_2(0)$ and $a_2(\infty)$. Therefore, the parity is stable in some range, which depends on the details of the spectral gap $\lambda_2 - \lambda_3$, the distance of parameters from a phase transition, and the angle between $\pi(T = 0)$, $\pi(T = \infty)$, and f_2 .

The above argument for stability can be explained using the geometric picture for the Mpemba effect that we discuss above. In any system, the $a_2 = 0$ hyperplane separates the probability space into two disjoint sets as we discuss in the three-state system above. The Boltzmann curve intersects the $a_2 = 0$ hyperplane at $T = T_b$. Any additional temperature T_M for which $a_2(T_M) = 0$ is an intersection between

the curve and the hyperplane, and \mathcal{I}_M counts these additional intersections. Topologically, the parity of the number of crossings between a continuous curve and a hyperplane of codimension one depends only on the boundaries of the equilibrium curve, namely, in our case on $\pi(T=0)$ and $\pi(T=\infty)$. If they are both on the same side of the hyperplane then the number of crossings is even, and if they are on different sides then the number of crossings is odd.

To appreciate the above topological aspect, let us contrast it with a (possibly only hypothetical) “superstrong Mpemba effect,” where there exists a temperature T_{SM} at which $a_2(T_{SM}) = a_3(T_{SM}) = a_4(T_{SM}) = 0$. In other words, consider a case where the coefficients of $\pi(T_{SM})$ vanish along ν_2 , ν_3 , and ν_4 . This implies an even faster relaxation than the strong effect. The condition for this superstrong effect $a_2(T_{SM}) = a_3(T_{SM}) = a_4(T_{SM}) = 0$ defines a hyperplane of codimension three that can intersect the probability simplex (which is of codimension one) in a codimension-two hyperplane. This hyperplane does not separate the space into two disjoint sets, and the topological argument does not work anymore. As an example of this fact, consider a codimension-two hyperplane in a 3D space, which is a straight line. It does not separate the 3D space into two disjoint sets as a plane does. Now consider an equilibrium locus that crosses the superstrong straight line in a 3D probability simplex. A small perturbation in the model parameters deforms the equilibrium locus a bit and generically separates the equilibrium locus from the straight line. Therefore, even an infinitesimal perturbation can (and usually does) destroy the superstrong Mpemba effect. In this sense, the strong Mpemba effect has topological stability, but the superstrong effect does not. We therefore do not expect to observe the superstrong effect in systems which are not fine-tuned.

IV. MEAN-FIELD ISING ANTIFERROMAGNETIC MODEL WITH GLAUBER DYNAMICS

The mechanism for the Mpemba effect suggested in Ref. [18] was so far demonstrated only in microscopic systems with a few degrees of freedom. However, all the experimental observations of similar effects are in macroscopic systems with a huge number of microstates. To discuss the applicability of the mechanism in such macroscopic systems, we next consider the Ising model with antiferromagnetic interactions and mean-field connectivity on a complete bipartite graph. This is a classical many-body model which has been studied extensively and whose phase diagram can be calculated exactly (see Fig. 6 in Ref. [25]). As we describe below, this model shows a rich Mpemba behavior, which survives the thermodynamic limit.

A. The model

In mean-field models, each spin interacts equally with all the other spins in the system. To generate a model of

antiferromagnetic interactions in the mean-field approximation, we consider a system with a total number of N spins, half of them on each “sublattice” or subgraph. Each spin interacts antiferromagnetically with all the spins in the other subgraph, but spins on the same subgraph do not interact at all. The interaction strength between the spins is fixed. This type of interaction can lead to an “antiferromagnetic phase” in which the spins in one sublattice are predominantly in the up state, while most spins in the other subgraph point down.

Let $N_{1,\uparrow}$, $N_{1,\downarrow}$ ($N_{2,\uparrow}$, $N_{2,\downarrow}$) be the number of spins pointing up and down on subgraph 1 (subgraph 2). We define the two magnetization densities on subgraphs 1 and 2 as

$$x_1 \equiv \frac{N_{1,\uparrow} - N_{1,\downarrow}}{N/2} \quad \text{and} \quad x_2 \equiv \frac{N_{2,\uparrow} - N_{2,\downarrow}}{N/2}. \quad (18)$$

Although the system has 2^N different microstates, all microstates that correspond to the same values of $N_{1,\uparrow}$ and $N_{2,\uparrow}$ are equivalent since the interaction strength is “position” independent (mean field). Thus, the Hamiltonian of this model is only a function of x_1 and x_2 and is given by

$$\mathcal{H} = \frac{N}{2} [-Jx_1x_2 - \mu H(x_1 + x_2)], \quad (19)$$

where J is the coupling constant, H is the external magnetic field, and μ is the magnetic moment. In the antiferromagnetic case, the coupling constant is negative $J < 0$, and for simplicity we choose the units such that $J = -1$ and $\mu = 1$.

The dynamics we consider for this model is Glauber dynamics, with only single spin-flip transitions allowed. Under this assumption, the rates of flipping a spin up or down in subgraphs 1 and 2 are given by

$$\begin{aligned} R^{u_1}(x_1, x_2) &= \frac{(1 - x_1)/2}{1 + e^{(-2x_2 - 2H)/T_b}}, \\ R^{u_2}(x_1, x_2) &= \frac{(1 - x_2)/2}{1 + e^{(-2x_1 - 2H)/T_b}}, \\ R^{d_1}(x_1, x_2) &= \frac{(1 + x_1)/2}{1 + e^{(2x_2 + 2H)/T_b}}, \\ R^{d_2}(x_1, x_2) &= \frac{(1 + x_2)/2}{1 + e^{(2x_1 + 2H)/T_b}}, \end{aligned} \quad (20)$$

where $R^{u_1}(x_1, x_2)$ is the rate of flipping a spin up in subgraph 1, and $R^{d_2}(x_1, x_2)$ is the rate of flipping a spin down in subgraph 2. The numerators in Eqs. (20) are the combinatorial factors that take into account how many spins can be flipped in the specific state of the system, and the denominator is the standard Glauber factor $1/(1 + e^{\beta_b \Delta E})$, where ΔE is the difference of energies before and after the spin flip [26].

B. Mpemba-index phase diagram

The Mpemba-index phase diagram of this model was calculated numerically for $N = 400$ and is shown in the upper panel of Fig. 2. At each point in the figure, that is, for each temperature T_b and magnetic field H of the environment, we calculate (numerically) the coefficient $a_2(T)$ of the slowest relevant eigenvector of the corresponding Glauber dynamics [Eq. (20)] at each point along the equilibrium line. From the monotonicity and zero crossing of these coefficients $a_2(T)$, we deduce what types of Mpemba effects exist at this point. The phase diagram in Fig. 2 is quite rich and has eight different phases differentiated through their colors, including regions with odd and even Mpemba index existing for the direct inverse or both effects.

To make sure that the observed phase diagram is not dominated by the number of spins in the system, we repeat this calculation with $N = 70$ and check that the phase diagram looks essentially the same (Fig. 2, lower panel). Moreover, we check other forms of rates—Metropolis and heat-bath dynamics, both with single spin flips only. Although the exact locations of the different phases are not identical in the different dynamics, the main features in the phase diagram are similar in all of them. An example for such a feature is the line at $H = 1$ across which the Mpemba phase changes. To explain this feature, we next consider the thermodynamic limit of this model.

C. The thermodynamic limit

Let us take the thermodynamic ($N \rightarrow \infty$) limit for the mean-field antiferromagnetic model described above. To this end, we first write explicitly the master equation using all the single flip rates. At the configuration (x_1, x_2) , a single spin in each subgraph can either flip from up to down or from down to up. Therefore, there are four different terms in the master equation corresponding to leaving the current configuration, and similarly, four transitions into the specific configuration:

$$\begin{aligned} \partial_t p(x_1, x_2) = & R^{u_1}(x_1 - \Delta x, x_2)p(x_1 - \Delta x, x_2) \\ & + R^{u_2}(x_1, x_2 - \Delta x)p(x_1, x_2 - \Delta x) \\ & + R^{d_1}(x_1 + \Delta x, x_2)p(x_1 + \Delta x, x_2) \\ & + R^{d_2}(x_1, x_2 + \Delta x)p(x_1, x_2 + \Delta x) \\ & - [R^{u_1}(x_1, x_2) + R^{d_1}(x_1, x_2) \\ & + R^{u_2}(x_1, x_2) + R^{d_2}(x_1, x_2)]p(x_1, x_2), \end{aligned} \quad (21)$$

where Δx is the change in the variable x due to a single spin flip. In the limit $N \rightarrow \infty$, we approximate x_1 and x_2 as continuous variables. Expanding both p and all the terms of R to first order in Δx , we get a Fokker-Planck-like equation

$$\partial_t p = \partial_{x_1} [(R^{d_1} - R^{u_1})p] + \partial_{x_2} [(R^{d_2} - R^{u_2})p]. \quad (22)$$

Note that in this case, there is no diffusion, as the corresponding term vanishes in the $N \rightarrow \infty$ limit. Hence, it originates from a Langevin equation without random noise, namely, from a deterministic equation for x_1 and x_2 . For such a deterministic motion, an initial distribution which is a (δ) function stays a (δ) function at all times, and it is therefore enough to know the evolution of the averages

$$\bar{x}_1(t) \equiv \int x_1 p(x_1, x_2) dx_1 dx_2, \quad (23)$$

$$\bar{x}_2(t) \equiv \int x_2 p(x_1, x_2) dx_1 dx_2. \quad (24)$$

Using these definitions, we write an “equation of motion” for the averages of \bar{x}_1 and \bar{x}_2 by substituting the values of the rates in Eq. (20) into Eqs. (22) and (23). After some algebra, these give

$$\begin{aligned} \dot{\bar{x}}_1 &= \frac{1}{2} \left(\tanh \frac{H - \bar{x}_2}{T_b} - \bar{x}_1 \right), \\ \dot{\bar{x}}_2 &= \frac{1}{2} \left(\tanh \frac{H - \bar{x}_1}{T_b} - \bar{x}_2 \right). \end{aligned} \quad (25)$$

Unfortunately, these equations are not always linearly stable: For some values of H , T_b , \bar{x}_1 , \bar{x}_2 , a small perturbation in the initial values of \bar{x}_1 , \bar{x}_2 changes the trajectory significantly. For example, when the initial condition has $\bar{x}_1 = \bar{x}_2$, the symmetry of the dynamic keeps \bar{x}_1 and \bar{x}_2 equal at all times, even if the equilibrium distribution which corresponds to the specific T_b and H is different. In such cases, any infinitesimal perturbation (in the initial condition or during the dynamic) results in relaxation towards the equilibrium rather than following the solution of the above equations. Fortunately, in a large fraction of the parameter space (H, T_b) , as well as in the vicinity of all the fixed points, the above equations are stable. When stable, these nonlinear equations describe the temporal evolution of the macroscopic system, and we can use them to understand the Mpemba behavior of the system.

Using the above result, let us look at the equilibrium locus in the thermodynamic limit. For each value of H and T_b , the equilibrium values of \bar{x}_1 , \bar{x}_2 , which we denote by ξ_1 , ξ_2 , are the steady state Eq. (25), namely, the solution of

$$\begin{aligned} 0 &= \tanh \frac{H - \xi_2}{T_b} - \xi_1, \\ 0 &= \tanh \frac{H - \xi_1}{T_b} - \xi_2. \end{aligned} \quad (26)$$

For each value of H , the equilibrium line can therefore be found using Eqs. (26) to calculate $\xi_1(T_b)$ and $\xi_2(T_b)$ for $0 \leq T_b \leq \infty$. Note that Eqs. (26) are symmetric to

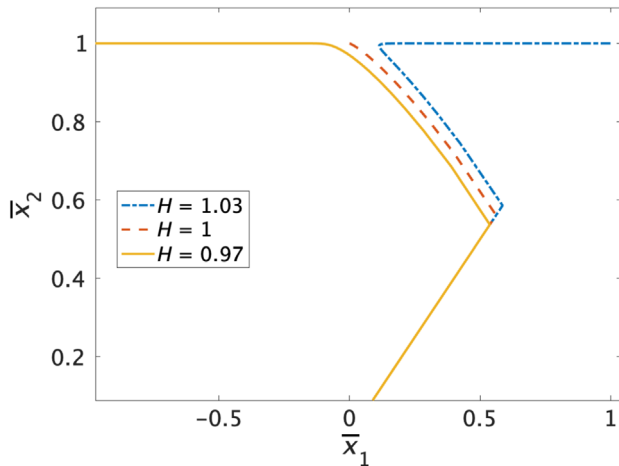


FIG. 3. The “equilibrium locus” of the mean-field antiferromagnetic Ising model at $H = 0.97$, $H = 1$, and $H = 1.03$ plotted in the plane of average magnetization densities in each subgraph \bar{x}_1 , \bar{x}_2 . Note the sharp transition in the curve’s shape around $H = 1$. This sharp transition corresponds to an abrupt transition in $a_2(T)$, which is clearly seen in the Mpemba-phase diagram in Fig. 2: The three equilibrium lines here correspond to the three dashed lines in the lower panel of Fig. 2.

exchanging \bar{x}_1 and \bar{x}_2 . We therefore limit ourselves, without loss of generality, to $\bar{x}_1 \leq \bar{x}_2$.

Examples for the equilibrium locus for $H = 0.99$, $H = 1$, and $H = 1.01$ are shown in Fig. 3, where for each T_b we numerically find the equilibrium by solving Eq. (26). As expected, at $T_b \rightarrow \infty$ both $\xi_1 \rightarrow 0$ and $\xi_2 \rightarrow 0$. Importantly, the equilibrium line is not a simple convex line; therefore, increasing the distance along the line does not necessarily increase the changes in the magnetizations. Moreover, at $H = 1$ the equilibrium locus has a singular transition demonstrated in Fig. 3. The sharp change in the equilibrium line at $H = 1$ corresponds to the first-order phase transition in the model at $H = 1$ when $T_b = 0$. This transition can be demonstrated by considering the limit $T_b \rightarrow 0$: For $H > 1$, the arguments of the hyperbolic tangents in Eq. (26) approach $+\infty$ asymptotically in the limit $T_b \rightarrow 0$, and hence, $\xi_{1,2} \rightarrow 1$. In contrast, for $H < 1$, $\xi_1 \rightarrow 1$ and $\xi_2 \rightarrow -1$ are the asymptotic solutions at $T_b \rightarrow 0$. As we discuss in Sec. III, this sharp transition in the shape of the equilibrium line naturally corresponds to the sharp transition in the Mpemba phases in Fig. 2: When the equilibrium locus abruptly changes, so does the coefficient along the slowest relaxation mode $a_2(T)$. Although this argument in principle should work only in the thermodynamic limit, it is evident from Fig. 2 that, in practice, it works well already at $N = 70$.

So far, we have seen that some features of the finite-system Mpemba-phase diagram can be explained using the thermodynamic limit. In the next section, we discuss the existence of Mpemba effects in the thermodynamic limit and their relations to the finite- N system.

D. Weak and strong Mpemba effects in the thermodynamic limit

For systems with a finite number of states and a given set of environmental parameters, we have a simple prescription to check what types of Mpemba effects exist: The monotonicity (weak effect) and zero crossings (strong effect) of the coefficient along the slowest dynamic $a_2(T)$ encapsulate all this information. In the thermodynamic limit, we cannot use the same method, as rarely does the coefficient $a_2(T)$ have an analytic expression at finite N , for which we can take the thermodynamic limit $N \rightarrow \infty$. Likewise, the direct calculation of $a_2(T)$ in the infinite system is often not feasible. This is somewhat unfortunate because all the experimental observations of Mpemba effects that we mention above are in macroscopic systems; hence, it is not clear that the mechanism we suggest is relevant for such systems. Moreover, the existence of the effect in macroscopic systems does not follow trivially from its existence in small systems. Although phase space becomes larger in large systems and thus more shortcuts may exist, in the thermodynamic limit, the probability distribution is concentrated in a tiny portion of the system’s phase space, which suggests that the system would rarely explore the extended phase space. Therefore, these shortcuts might not be as relevant.

Although we cannot use $a_2(T)$ to analyze the existence of Mpemba effects in the thermodynamic limit of the antiferromagnetic Ising model, for any environmental conditions (T_b, H) and two temperatures T_h and T_c , Eq. (25) can be used to compare the relaxation trajectories initiated from the corresponding equilibrium distributions. A natural and physically motivated distance function in this case is the free-energy difference between the current state and the equilibrium state, namely,

$$D[(\bar{x}_1, \bar{x}_2), (\xi_1, \xi_2)] = \mathcal{F}(\bar{x}_1, \bar{x}_2) - \mathcal{F}(\xi_1, \xi_2), \quad (27)$$

where the free energy is given by [25]

$$\begin{aligned} \mathcal{F}(x_1, x_2) = & \frac{\mathcal{H}(x_1, x_2)}{N} + \frac{T_b}{4}(1+x_1)\log(1+x_1) \\ & + \frac{T_b}{4}(1-x_1)\log(1-x_1) \\ & + \frac{T_b}{4}(1+x_2)\log(1+x_2) \\ & + \frac{T_b}{4}(1-x_2)\log(1-x_2), \end{aligned} \quad (28)$$

and $\mathcal{H}(x_1, x_2)$ is given by Eq. (19). If the initial condition with a longer distance from the equilibrium becomes, after some finite time, closer to equilibrium, then we know that there is a Mpemba effect in this system. However, checking if a Mpemba effect exists at a point using this approach is tedious—it requires solving the relaxation trajectories for all initial conditions. Luckily, checking if strong effects

exist and identifying their index is a much easier task. To this end, we can linearize Eqs. (25) near the equilibrium point corresponding to (T_b, H) . Denoting the differences from the equilibrium by $\Delta x_i = \xi_i - \bar{x}_i$, we can write for small Δx_i ,

$$\Delta \dot{x}_1 = \frac{\beta_b(1 - \xi_1^2)\Delta x_2 - \Delta x_1}{2} + \mathcal{O}(\Delta x_i^2), \quad (29)$$

$$\Delta \dot{x}_2 = \frac{\beta_b(1 - \xi_2^2)\Delta x_1 - \Delta x_2}{2} + \mathcal{O}(\Delta x_i^2). \quad (30)$$

These linearized equations have two relaxation eigendirections: a fast direction and a slow direction, with relaxation rates given by

$$\bar{\lambda}_1 = -\frac{1}{2} \left(1 - \beta_b \sqrt{(1 - \xi_1^2)(1 - \xi_2^2)} \right), \quad (31)$$

$$\bar{\lambda}_2 = -\frac{1}{2} \left(1 + \beta_b \sqrt{(1 - \xi_1^2)(1 - \xi_2^2)} \right). \quad (32)$$

Unless the initial condition is such that at the long time limit the coefficient of points on its trajectory along the slow direction (namely, the eigenvector corresponding to $\bar{\lambda}_1$) is zero, at long enough time the relaxation is from the direction corresponding to the slow direction. The number of trajectories that start on the equilibrium locus and approach the equilibrium point asymptotically from the fast direction is the Mpemba index, and the corresponding initial conditions show strong Mpemba effect. To find if such initial conditions exist, we can propagate backwards in time solutions to Eqs. (25) that approach the equilibrium from the fast direction (there are two such trajectories; one from each side of the equilibrium locus). The number of crossings between these shoot-back trajectories and the equilibrium locus is the Mpemba index.

As an example, consider the relaxation dynamic for an environment with $H = 1.1$ and $T_b = 0.5$. The equilibrium locus as well as the relaxation trajectories from different initial temperatures are plotted in the upper panel of Fig. 4. As can be seen in the figure, there is a “fast” and a “slow” direction to the relaxation process, and essentially all the trajectories relax to equilibrium from the slow direction—except for a single trajectory (the red dashed trajectory) that relaxes directly from the fast direction. This special trajectory is the strong inverse Mpemba with $\mathcal{I}_M = 1$, in agreement with the finite-state phase diagram in Fig. 2 for these values of H and T_b . In this case, the ratio between the relaxation rates $\bar{\lambda}_1$ and $\bar{\lambda}_2$ given in Eq. (31) is 14.7. In other words, not only does the strong Mpemba initial condition relax exponentially faster, the relaxation rate is an order of magnitude higher than that from any other initial temperature. Indeed, as shown in Fig. 5, the strong effective trajectory relaxes significantly faster towards the equilibrium compared to all the other initial temperatures.

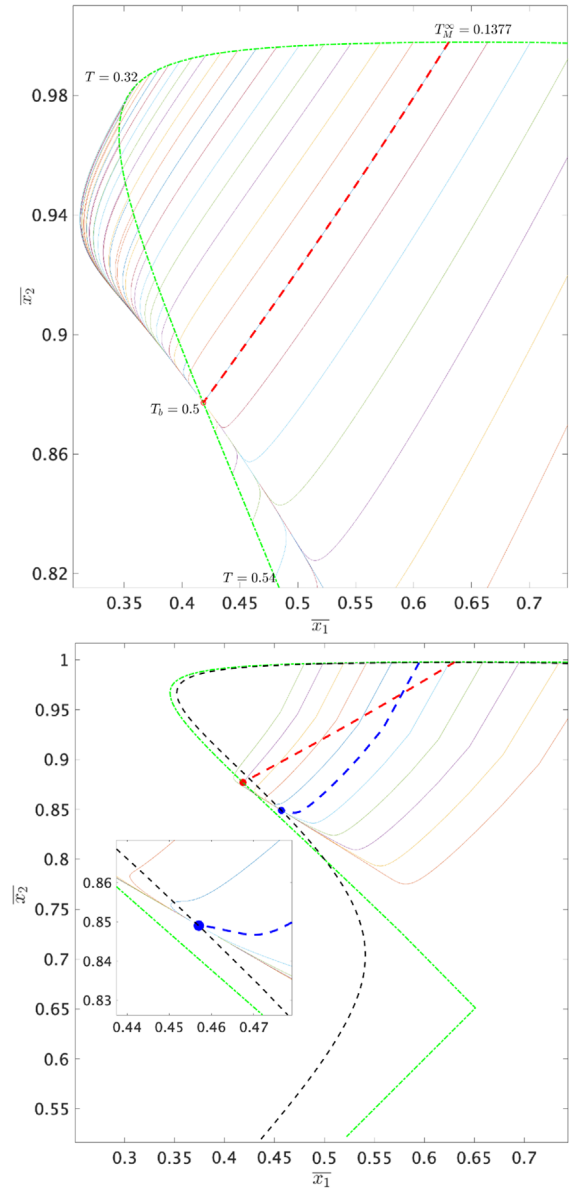


FIG. 4. Upper panel: The thick green dashed line is the equilibrium locus, and the colored lines are the relaxation trajectories toward the equilibrium point (the red circle). All relaxation trajectories except the dashed red one approach equilibrium from the slow direction. The red dashed trajectory approaches equilibrium from the fast direction, and it corresponds to the strong inverse Mpemba trajectory (with bath temperature $T_b = 0.5$ and initial temperature $T_M^\infty = 0.1377$). Its relaxation rate is 14.7 times faster than the other trajectories; see Fig. 5. Lower panel: A comparison between the thermodynamic limit and finite system with $N = 400$. The dash-dot thick green line is the thermodynamic limit equilibrium line, and the dashed black line is the projection into (\bar{x}_1, \bar{x}_2) of the equilibrium line in the finite system. The projections of the relaxation trajectories for several initial temperatures are shown as thin lines, and the relaxation which corresponds to the strong Mpemba [calculated by $a(T_M) = 0$] is the thick blue dashed line. The inset shows an enlargement of the relaxation trajectories near the equilibrium. The strong Mpemba initial condition approaches equilibrium from a different direction.

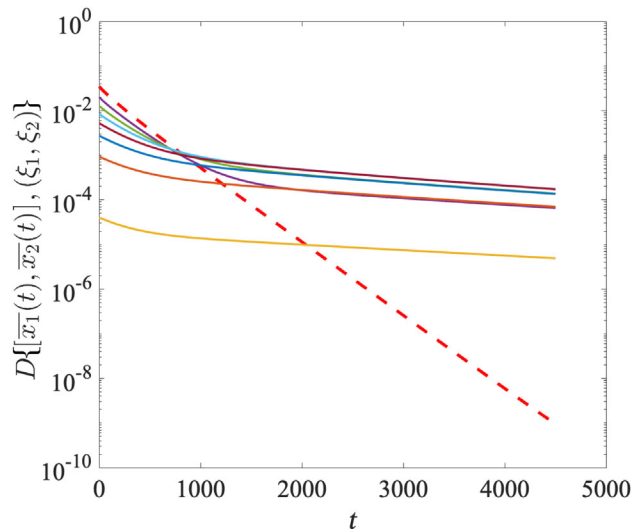


FIG. 5. The distance from equilibrium [defined in Eq. (27)] in logarithmic scale as a function of time for several initial conditions in the thermodynamic limit. The initial condition corresponding to the strong effect is the dashed line.

E. Comparing the thermodynamic limit with a finite- N system size

So far, we have seen the strong Mpemba effect in both the finite state $N = 400$ and the thermodynamic limit of the antiferromagnetic mean-field Ising model. However, it is not obvious that the two effects are trivially related: In the thermodynamic limit, the effect is derived by linearizing the nonlinear equations for the order parameters, Eqs. (25), not by considering $a_2(T)$ in the $N \rightarrow \infty$ limit, which is intractable. One way to compare the two cases is to calculate a Mpemba-phase diagram for the thermodynamic limit and compare it with Fig. 2. However, in the paramagnetic phase ($\bar{x}_1 = \bar{x}_2$), we cannot use Eqs. (25) as they are not linearly stable, as we discuss above. Therefore, we perform instead several other comparisons as presented next.

One hint that the two effects are nevertheless related is the sharp transition of the equilibrium line at $H = 1$ and the corresponding jump in the Mpemba index shown in Fig. 2 and discussed above. To further convince that the strong Mpemba effect in the thermodynamic limit corresponds to the finite-system case, the temperature at which a strong effect occurs $T_M(N)$ is calculated for various values of system size N . Figure 6 shows that indeed $T_M(N)$ converges at the large- N limit to the temperature T_M^∞ at which a strong effect occurs in the thermodynamic limit for the chosen T_b and H . Similar behavior is observed in a wide range of temperatures and magnetic fields.

Additional comparison between a finite system and the thermodynamic limit is shown in the lower panel of Fig. 4. For $N = 400$, we calculate the equilibrium distribution as a function of the temperature and “project” it into the (\bar{x}_1, \bar{x}_2) plane by calculating the equilibrium-averaged magnetization in each sublattice. This equilibrium line is given by the

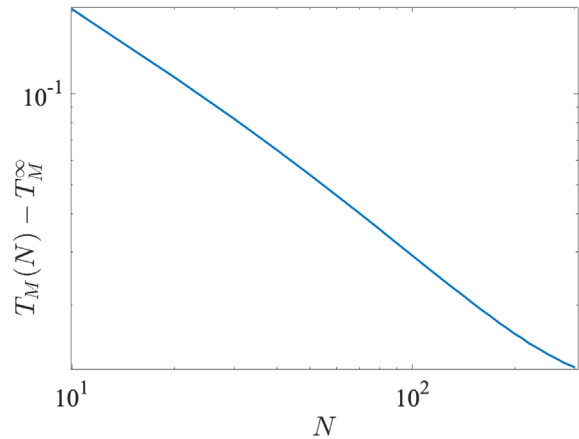


FIG. 6. Comparison between the strong effect in the N spin system and the strong effect in the thermodynamic limit. The temperature from which there is a strong effect on the finite- N system $T_M(N)$ converges to the temperature from which there is a strong effect in the thermodynamic limit T_M^∞ .

thick black dashed line in the figure. For comparison, the green dash-dotted line is the thermodynamic limit equilibrium line, as in the upper panel. Next, we calculate the probability distribution dynamics initiated at several Boltzmann distributions of temperatures in the range $T \in [0.1, 0.2]$. This is done using Eq. (1), with R defined in Eq. (20). These trajectories in probability space are projected to the (\bar{x}_1, \bar{x}_2) plane and are shown by the colored thin lines. Lastly, the trajectory of the strong effect $T_M = 0.148$ that solves $a_2(T_M) = 0$ is calculated too and is plotted by the thick blue dashed line. For comparison, the strong Mpemba trajectory in the thermodynamic limit initiated at $T_M^\infty = 0.1377$ is plotted as a thick dashed red line. As shown in the inset, all the trajectories except the strong Mpemba effect approach the equilibrium point (the blue circle) from the slow direction, and the strong effect approaches the equilibrium point from a different fast direction. Note that the equilibrium line and the trajectories in the thermodynamic limit are not identical to those of the finite system, hinting that $N = 400$ is not large enough to match the thermodynamic limit. Nevertheless, this example demonstrates that the $a_2(T_M) = 0$ in finite-size systems maps into the strong Mpemba mechanism in the thermodynamic limit. Although not mathematical proof, this analysis hints that the strong Mpemba effect in the thermodynamic limit is a consequence of the strong effect in the finite system.

F. Temperature overshooting during relaxation

As we discuss above, the existence of a Mpemba effect can be checked by calculating the distance from equilibrium as a function of time from two different initial points on the equilibrium lines. This requires a choice of some reasonable distance function, e.g., the free-energy distance [see Eq. (27)]. In the specific case of the mean-field

antiferromagnetic model, there is another natural option: Even though the system is not in equilibrium through relaxation, it is possible to associate a temperature with each state during the relaxation process and use this temperature to compare different relaxations. This temperature does not have all the properties commonly required from a distance function, e.g., it is not monotonically decreasing in a relaxation; nevertheless, it sheds light on additional counterintuitive aspects of thermal relaxations far from equilibrium. As we show below, the temperature can overshoot the environment temperature. In other words, a hot system when coupled to a cold bath can reach during its relaxation process temperatures which are *lower* than the environment's temperature.

To associate a temperature for each point in the relaxation process, let us use the following coordinate transformation from (\bar{x}_1, \bar{x}_2) to $(T_{\text{eq}}, H_{\text{eq}})$ defined by

$$\begin{aligned} H_{\text{eq}} &\equiv \frac{\bar{x}_1 \tanh^{-1} \bar{x}_1 - \bar{x}_2 \tanh^{-1} \bar{x}_2}{\tanh^{-1} \bar{x}_1 - \tanh^{-1} \bar{x}_2}, \\ T_{\text{eq}} &\equiv \frac{\bar{x}_1 + \bar{x}_2}{\tanh^{-1} \bar{x}_1 - \tanh^{-1} \bar{x}_2}. \end{aligned} \quad (33)$$

The physical significance of this transformation can be understood by a simple algebraic manipulation of the above equations that gives Eq. (26). Comparing these to Eq. (25), one notes that for an environment with temperature $T_b = T_{\text{eq}}$ and external magnetic field $H = H_{\text{eq}}$, the specific state given by (\bar{x}_1, \bar{x}_2) is the equilibrium. In other words, if during the relaxation process when the system is in the state (\bar{x}_1, \bar{x}_2) , the system is decoupled from the current environment and coupled to a different environment with $T_b = T_{\text{eq}}$ and $H = H_{\text{eq}}$, then the system would be in equilibrium with the new environment. It is therefore natural to interpret H_{eq} and T_{eq} as the magnetic field and temperature of the system itself.

Before proceeding, two comments on the above mapping are in order. (i) Note that the transformation is singular at $\bar{x}_1 = \bar{x}_2$ as the denominator in Eqs. (33) vanishes. In other words, we cannot associate a single temperature and magnetic field for states in which $\bar{x}_1 = \bar{x}_2$. (ii) The ability to associate the equilibrium temperature and magnetic field to most states of the system is a very nongeneric property. It is a consequence of the fact that the number of parameters in the model is identical to the number of order parameters describing the system in the thermodynamic limit. Luckily, in the thermodynamic limit of this model, the probability distribution becomes a δ function with exactly two order parameters.

Using the mapping in Eq. (33), we plot in Fig. 7 the temperature of the system as a function of time for various initial conditions along the equilibrium line. As can be seen, not only do the temperature curves cross—namely, a Mpemba effect occurs—but also for some relaxation trajectories the temperature is nonmonotonic as a function

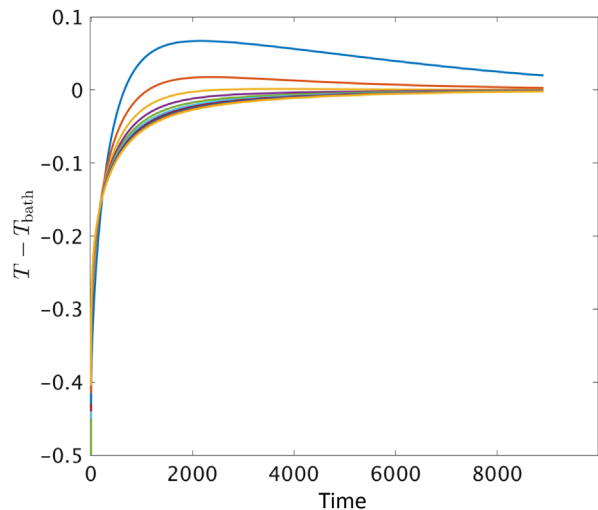


FIG. 7. $T_{\text{eq}} - T_{\text{bath}}$ as a function of time for various initial temperatures along the equilibrium line. The inverse Mpemba effect is shown here as a crossing of two curves—initially, the colder system heats up faster. The figure also shows that the temperature can overshoot the environment temperature—the system can reach equilibrium temperatures which are higher than that of the environment.

of time. Moreover, systems that are initiated at temperatures lower than the environment's temperature can reach temperatures which are higher than that of the environment in their relaxation. Similar nonmonotonic relaxations were discussed in the context of non-Markovian thermal relaxation [27] or finite baths [28], but as far as we know, this is the first example for such a nonmonotonic relaxation in Markovian dynamics and in the thermodynamic limit.

It is interesting to note that the temperature overshoot is tightly connected with the strong Mpemba effect. To explain this, let us examine Fig. 4 carefully. Initial temperatures to the left of the strong Mpemba relaxation trajectory approach equilibrium from one side of the slow direction, and initial temperatures to the right of the strong Mpemba trajectory approach equilibrium from the opposite direction, which is also a slow direction. Opposite directions mean opposite directions in the coordinate T_{eq} ; namely, there are trajectories that approach equilibrium from both higher and lower temperatures compared to the environment. Conversely, if there are trajectories that approach equilibrium from both higher and lower temperatures, they must approach equilibrium from opposite directions of the slow relaxation. Therefore, by continuity there must also be a trajectory that approaches equilibrium from the fast direction, and this trajectory corresponds to a strong effect.

V. HOW GENERIC IS THE MPEMBA EFFECT IN THE REM MODEL?

So far, we have considered the Mpemba effect in a specific model—the mean-field antiferromagnetic Ising

model. Is the existence of the Mpemba effect a special property of this model, or should we expect to see similar effects in many other models? To address this question, we next evaluate the probability of having a Mpemba effect in a class of models with random parameters. As we discuss below, the strong Mpemba effect plays a crucial role in our ability to estimate the probability of having a Mpemba effect.

A. Analytical estimates: The isotropic ensemble

A proper analysis of the probability to find a Mpemba effect in classes of random models is a formidable challenge: One must perform the rather difficult calculation of the second eigenvector \mathbf{f}_2 and the coefficient a_2 in Eq. (11) as a function of the initial temperature, the energies, and the barriers and then average over the ensemble. Even the simpler problem of analyzing the strong Mpemba effect requires facing the daunting task of analyzing the number of zeros in Eq. (11).

To gain some analytical insight, we proceed by estimating the strong Mpemba probability in an ensemble of relaxation dynamics which we call the isotropic ensemble. The ensemble is chosen to represent a wide distribution of barriers so that the distribution of eigenvectors of the relaxation modes is as isotropic as possible, consistent with a given target thermal distribution. Explicitly, given a set of L energies $\{E_1, E_2, \dots, E_L\}$, we average over an ensemble of random \mathbf{f}_2 eigenvectors that are orthogonal, in the sense of the quadratic form in Eq. (11), to the equilibrium distribution with a given bath temperature T_b . This approach allows us to perform analytically the ensemble averaging. We then compare our analytic results for the isotropic ensemble with direct numerical calculations on the matrix Eq. (4) with fixed energies and random barriers and find surprisingly good agreement in certain parameter regimes.

For a given set of energies E_1, \dots, E_L and dynamics prescribed by the Markov matrix Eq. (4), the steady-state distribution is the Boltzmann distribution at T_b : $\boldsymbol{\pi}(T_b)$. The first eigenvector of the symmetrized Markov matrix \tilde{R} is

$$\mathbf{f}_1 \equiv F^{1/2} \boldsymbol{\pi}(T_b) = \frac{1}{Z(T_b)} (e^{-[(\beta_b E_1)/2]}, \dots, e^{-[(\beta_b E_L)/2]}) \quad (34)$$

and $\tilde{R}\mathbf{f}_1 = \mathbf{0}$. The second eigenvector of \tilde{R} , \mathbf{f}_2 together with the initial condition $\boldsymbol{\pi}(T)$ determine the coefficient a_2 , which according Eq. (11) is

$$a_2(T) = \sum_{i=1}^L \frac{(\mathbf{f}_2)_i e^{-[\beta - (\beta_b/2)]E_i}}{\|\mathbf{f}_2\|^2 Z(T)}. \quad (35)$$

We obtain the explicit expression for the parity of the direct Mpemba index as a function of \mathbf{f}_2 by plugging Eq. (35) into Eq. (15) and find

$$\begin{aligned} \mathcal{P}(\mathcal{I}_M^{\text{dir}}) &= \theta \left(\left[\sum_{j=1}^L (\mathbf{f}_2)_j e^{-[(\beta_b E_j)/2]} (\langle E \rangle_b - E_j) \right] \right. \\ &\quad \left. \times \left[\sum_{i=1}^L (\mathbf{f}_2)_i e^{[(\beta_b E_i)/2]} \right] \right), \end{aligned} \quad (36)$$

where $\langle E \rangle_b \equiv \sum_{i=1}^L E_i e^{-\beta_b E_i} / Z(T_b)$ is the average energy in equilibrium at T_b . We can represent Eq. (36) in the form

$$\mathcal{P}(\mathcal{I}_M^{\text{dir}}) = \theta[(\mathbf{f}_2 \cdot \mathbf{u}^{\text{dir}})(\mathbf{f}_2 \cdot \mathbf{w})], \quad (37)$$

with the vectors \mathbf{u}^{dir} and \mathbf{w} defined as

$$(\mathbf{u}^{\text{dir}})_i \equiv e^{[(\beta_b E_i)/2]}, \quad (38)$$

$$(\mathbf{w})_i \equiv e^{-\frac{\beta_b E_i}{2}} (\langle E \rangle_b - E_i). \quad (39)$$

Note that the vectors \mathbf{u}^{dir} and \mathbf{w} appearing in this form depend solely on the set of energies and on the bath temperature—they are independent of the barriers. Moreover, the form of Eq. (37) has a simple geometric meaning. To see it, we single out the components of \mathbf{f}_2 in the plane spanned by the (nonorthogonal) vectors \mathbf{u}^{dir} , \mathbf{w} . Choosing f_{\parallel} as the component of \mathbf{f}_2 parallel to \mathbf{u}^{dir} , we have

$$\begin{aligned} \mathbf{f}_2 &= f_{\parallel} \frac{\mathbf{u}^{\text{dir}}}{\|\mathbf{u}^{\text{dir}}\|} + f_{\perp} \frac{(\mathbf{w} - \frac{\mathbf{w} \cdot \mathbf{u}^{\text{dir}}}{\|\mathbf{u}^{\text{dir}}\|^2} \mathbf{u}^{\text{dir}})}{\sqrt{\|\mathbf{w}\|^2 - \frac{(\mathbf{w} \cdot \mathbf{u}^{\text{dir}})^2}{\|\mathbf{u}^{\text{dir}}\|^2}}} \\ &\quad + \text{terms orthogonal to } \mathbf{u}^{\text{dir}} \text{ and } \mathbf{w}. \end{aligned} \quad (40)$$

In this basis, $(\mathbf{f}_2 \cdot \mathbf{u}^{\text{dir}})(\mathbf{f}_2 \cdot \mathbf{w})$ is equal to

$$\begin{aligned} &(\mathbf{f}_2 \cdot \mathbf{u}^{\text{dir}})(\mathbf{f}_2 \cdot \mathbf{w}) \\ &= f_{\parallel}^2 (\mathbf{u}^{\text{dir}} \cdot \mathbf{w}) + f_{\parallel} f_{\perp} |\mathbf{u}^{\text{dir}} \cdot \mathbf{w}| K(\mathbf{u}^{\text{dir}}, \mathbf{w}), \end{aligned} \quad (41)$$

where

$$K(\mathbf{u}^{\text{dir}}, \mathbf{w}) \equiv \sqrt{\frac{\|\mathbf{u}^{\text{dir}}\|^2 \|\mathbf{w}\|^2}{(\mathbf{w} \cdot \mathbf{u}^{\text{dir}})^2} - 1}. \quad (42)$$

Therefore, on the f_{\parallel} , f_{\perp} plane, the region satisfying $\mathcal{P}(\mathcal{I}_M^{\text{dir}}) \neq 0$ is a double wedge

$$f_{\parallel}^2 (\mathbf{u}^{\text{dir}} \cdot \mathbf{w}) + f_{\parallel} f_{\perp} |\mathbf{u}^{\text{dir}} \cdot \mathbf{w}| K > 0 \quad (43)$$

(see Fig. 8). The boundary of the region is associated with the lines $f_{\perp} = -f_{\parallel}/K$ and $f_{\parallel} = 0$.

The same treatment is also possible for the inverse Mpemba effect. For example, assuming, for simplicity, a nondegenerate ground state and ordering the energies so

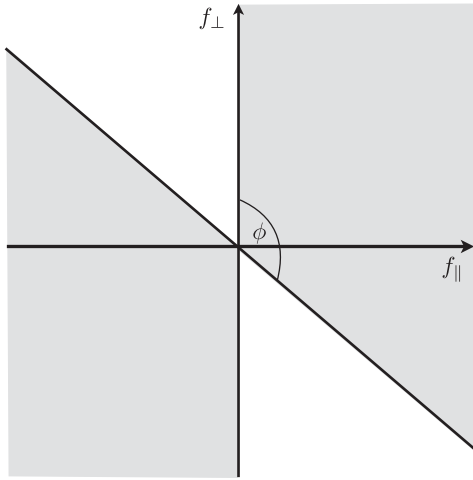


FIG. 8. The direct Mpemba index $\mathcal{I}_M^{\text{dir}}$ is odd in the double-wedge shaded region of the $f_{\parallel}f_{\perp}$ plane if $\mathbf{u}_2^{\text{dir}} \cdot \mathbf{w} > 0$, and while if $\mathbf{u}_2^{\text{dir}} \cdot \mathbf{w} < 0$, the direct Mpemba index is odd for the complementary region (white). See Eq. (43).

that E_1 is the ground-state energy, we find that $\mathcal{P}(\mathcal{I}_M^{\text{inv}})$ is given by Eq. (37) with the replacement

$$\mathbf{u}^{\text{dir}} \rightarrow \mathbf{u}^{\text{inv}}; \quad (\mathbf{u}^{\text{inv}})_i = -e^{[(\beta_b E_i)/2]} \delta_{i,1}. \quad (44)$$

Next, we formulate the averaging over the admissible \mathbf{f}_2 vectors. In the class of random relaxations we consider, we generate \mathbf{f}_2 by picking a random vector $\mathbf{g} = (g_1, \dots, g_L)$ and obtaining from it a random vector orthogonal to \mathbf{f}_1 (by subtracting the projection of \mathbf{g} on \mathbf{f}_1)

$$\mathbf{f}_2(\mathbf{g}) \equiv \mathbf{g} - \frac{\mathbf{g} \cdot \mathbf{f}_1}{\|\mathbf{f}_1\|^2} \mathbf{f}_1. \quad (45)$$

The distribution of the \mathbf{g} vectors is taken to be isotropic, and therefore, the projection of the distribution of the \mathbf{g} 's onto the hyperplane orthogonal to \mathbf{f}_1 is also isotropic. For this purpose, we take the g_i 's in \mathbf{g} to be IID Gaussian variables. Analogous to the derivation of Eq. (37), we plug Eq. (45) into Eq. (36) and separate the g_i components. We find that the direct Mpemba parity for a particular realization of g_i can be written as

$$\mathcal{P}(\mathcal{I}_M^{\text{dir}}) = \theta[(\mathbf{g} \cdot \mathbf{u}_{\text{iso}}^{\text{dir}})(\mathbf{g} \cdot \mathbf{w})], \quad (46)$$

where \mathbf{w} is defined in Eq. (39) and $\mathbf{u}_{\text{iso}}^{\text{dir}}$ is given by

$$(\mathbf{u}_{\text{iso}}^{\text{dir}})_i = e^{[(\beta_b E_i)/2]} - \frac{L e^{-[(\beta_b E_i)/2]}}{Z(T_b)}, \quad (47)$$

where L is the number of energy levels (or the system size). As before, we break \mathbf{g} into the components parallel and perpendicular to $\mathbf{u}_{\text{iso}}^{\text{dir}}$ and find as before

$$(\mathbf{g} \cdot \mathbf{u}_{\text{iso}}^{\text{dir}})(\mathbf{g} \cdot \mathbf{w}) \quad (48)$$

$$= g_{\parallel}^2 (\mathbf{u}_{\text{iso}}^{\text{dir}} \cdot \mathbf{w}) + g_{\parallel} g_{\perp} |\mathbf{u}_{\text{iso}}^{\text{dir}} \cdot \mathbf{w}| K(\mathbf{u}_{\text{iso}}^{\text{dir}}, \mathbf{w}), \quad (49)$$

where K is defined in Eq. (42).

The Gaussian IID's g_i have a rotationally invariant joint distribution function, and therefore, in any coordinate system the components are corresponding Gaussian IID's. It follows that g_{\parallel}, g_{\perp} are Gaussian IID's and have a rotationally invariant distribution on the g_{\parallel}, g_{\perp} plane. On this plane, the region satisfying $\mathcal{P}(\mathcal{I}_M^{\text{dir}}) > 0$ is a double wedge (cf. Fig. 8), and the probability of g_{\parallel}, g_{\perp} to fall inside the wedge depends only on the wedge angle.

Geometrically, if ϕ is the angle between \mathbf{u} and \mathbf{w} , then $\text{Prob}[\mathcal{P}(\mathcal{I}_M^{\text{dir}}) > 0] = (\phi/\pi)$ when $(\mathbf{u} \cdot \mathbf{w}) > 0$ [and $\text{Prob}[\mathcal{P}(\mathcal{I}_M^{\text{dir}}) > 0] = 1 - (\phi/\pi)$ when $(\mathbf{u} \cdot \mathbf{w}) < 0$]. Expressed explicitly in terms of $\mathbf{u}_{\text{iso}}^{\text{dir}}, \mathbf{w}$ we find

$$\text{Prob}[\mathcal{P}(\mathcal{I}_M^{\text{dir}}) > 0] = \frac{1}{2} + \frac{\text{sign}(\mathbf{u}_{\text{iso}}^{\text{dir}} \cdot \mathbf{w})}{\pi} \arctan \frac{1}{K(\mathbf{u}_{\text{iso}}^{\text{dir}}, \mathbf{w})}. \quad (50)$$

To recap, the formula Eq. (50) represents, for a given set of energies $\{E_i\}$ and bath temperature T_b , the probability that the direct Mpemba index is odd.

Equation (50) can be simplified for hot bath temperatures $k_B T_b \gg \max(\{E_1, \dots, E_L\})$, and asymptotically it gives

$$\text{Prob}[\mathcal{P}(\mathcal{I}_M^{\text{dir}}) > 0] \approx \frac{C_E}{T_b}. \quad (51)$$

Here, the constant C_E depends only on the first few moments of the energy level distribution (for the explicit expression, see the Appendix A).

Figure 9 shows a comparison of Eq. (50) with a random realization of $L = 15$ energies and Mpemba index averaged over 4000 realizations of random barriers. The expression seems to capture surprisingly nicely the behavior of a random draw of energy levels when the barriers' distribution is wider than the distribution of energies and the temperature is higher than the characteristic energy spread.

Similarly, for the inverse Mpemba effect we have

$$\mathcal{P}(\mathcal{I}_M^{\text{inv}}) = \theta[(\mathbf{g} \cdot \mathbf{u}_{\text{iso}}^{\text{inv}})(\mathbf{g} \cdot \mathbf{w})], \quad (52)$$

where \mathbf{w} is defined in Eq. (39), and $\mathbf{u}_{\text{iso}}^{\text{inv}}$ is given by

$$(\mathbf{u}_{\text{iso}}^{\text{inv}})_i = -e^{[(\beta_b E_i)/2]} \delta_{i,1} + \frac{e^{-[(\beta_b E_i)/2]}}{Z(T_b)}, \quad (53)$$

where we assume that E_1 is the lowest energy. As before,

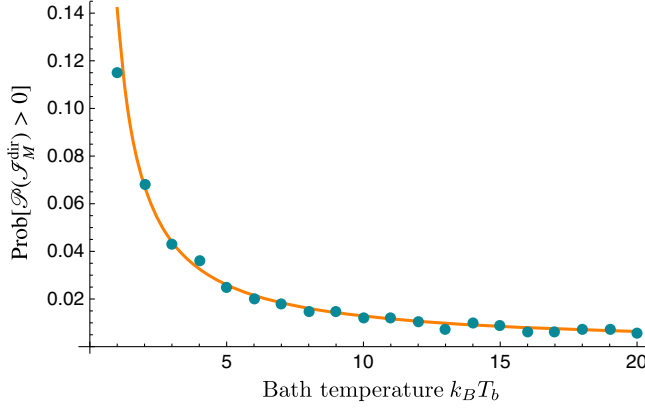


FIG. 9. The probability for the odd direct Mpemba index for a particular random draw of $L = 15$ energy levels obtained two independent ways: analytically by averaging over the isotropic ensemble (solid line) and numerically by averaging over random barriers (points). The energy level realization is drawn from a Gaussian distribution with zero mean and standard deviation 1.5. Each point corresponds to the average of 4000 barrier realizations taken from a truncated Gaussian distribution with zero mean and standard deviation 15 (the Gaussian is truncated to have only positive B_{ij} values). The solid line represents the analytical result for the isotropic ensemble Eq. (50).

$$\text{Prob}[\mathcal{P}(\mathcal{I}_M^{\text{inv}}) > 0] = \frac{1}{2} + \frac{\text{sign}(\mathbf{u}_{\text{iso}}^{\text{inv}} \cdot \mathbf{w})}{\pi} \arctan \frac{1}{K(\mathbf{u}_{\text{iso}}^{\text{inv}}, \mathbf{w})}. \quad (54)$$

Substituting for \mathbf{w} and $\mathbf{u}_{\text{iso}}^{\text{inv}}$ from Eqs. (39) and (53), we get

$$\mathcal{P}(\mathcal{I}_M^{\text{inv}}) = \frac{1}{2} - \frac{1}{\pi} \arctan \left(\frac{1}{\sqrt{\frac{[Z(T_b)e^{\beta_b E_1} - 1] \Delta E_b^2}{(E_1 - E_b)^2} - 1}} \right). \quad (55)$$

The above expression simplifies in the limit of a very low bath temperature $k_B T_b \ll (E_2 - E_1)$. Without loss of generality, we set $E_1 = 0$ and obtain

$$\text{Prob}[\mathcal{P}(\mathcal{I}_M^{\text{inv}}) > 0] \approx \frac{1}{2} - \frac{1}{\pi} \arctan \left(\sqrt{\frac{(E_2 \varepsilon_2 + E_3 \varepsilon_3)^2}{(E_2 - E_3)^2 \varepsilon_2 \varepsilon_3 (1 + \varepsilon_2 + \varepsilon_3)}} \right). \quad (56)$$

Simplifying the expression even further, we get

$$\text{Prob}[\mathcal{P}(\mathcal{I}_M^{\text{inv}}) > 0] \approx \frac{1}{\pi} \sqrt{\frac{(E_2 - E_3)^2 \varepsilon_2 \varepsilon_3 (1 + \varepsilon_2 + \varepsilon_3)}{(E_2 \varepsilon_2 + E_3 \varepsilon_3)^2}}, \quad (57)$$

where $\varepsilon_i \equiv e^{-\beta_b E_i}$. Taking $\varepsilon_3 \rightarrow 0$ or if $E_2 = E_3$, we find

$$\text{Prob}[\mathcal{P}(\mathcal{I}_M^{\text{inv}}) > 0] \approx 0, \quad (58)$$

which is expected, as there is no Mpemba effect for a two-level system.

It is important to note that the isotropic ensemble, while introduced for the purpose of enabling analytical averaging, is consistent with the assumptions of our relaxation dynamics. Namely, one can prove the following theorem.

Theorem 1.—Given any choice of a real vector \mathbf{f}_2 orthogonal to \mathbf{f}_1 in Eq. (34), there exists a set of barriers B_{ij} with relaxation dynamics obeying detailed balance (4) having $F^{-1/2} \mathbf{f}_2$ as its slowest relaxation eigenvector.

The proof can be found in Appendix B.

B. Numerically: The probability of the strong Mpemba effect in the REM model

In the previous section, we analyze an analytically tractable model; however, in general, estimating the probability of the Mpemba effect is a daunting and often impossible task. In what follows, we numerically study the probability of having a strong Mpemba effect in the REM.

The random energy model was introduced by Derrida as an extreme limit of spin glasses [29]. It is the simplest model of a system with quenched disorder that has a phase transition. In the REM, L energy levels are IID random variables. The conventional choice for the probability distribution of E_j 's is a Gaussian distribution

$$\text{Prob}(E_j = E) = \frac{1}{\sqrt{2\pi\sigma_E^2 \log_2 L}} e^{-[E^2/(2\sigma_E^2 \log_2 L)]}, \quad (59)$$

where in order to have extensive thermodynamic potentials, the variance depends on the system size. At temperatures lower than $T_{\text{critical}} \equiv \sigma_E / (k_B \sqrt{2 \ln 2})$, the system is trapped in a few low-lying states; this condensation phenomena is a phase transition, and at the transition the free energy is nonanalytic.

Note that quenched disorder is not necessary for the Mpemba effect. Our previous examples, such as the mean-field Ising antiferromagnet and other examples discussed in Ref. [18] are proof that quenched disorder is not an essential feature for this effect.

The Mpemba effect is a property of the system and its dynamics; thus, to study it, we need to specify the barriers B_{ij} in Eq. (4). Here we chose B_{ij} as IID random variables obeying a ‘‘truncated’’ Gaussian distribution

$$\text{Prob}(B_{ij} = B) = \frac{1}{\sqrt{2\pi\sigma_B^2 \log_2 L}} e^{-[B^2/(2\sigma_B^2 \log_2 L)]} \theta(B), \quad (60)$$

and θ is the Heaviside step function. This particular choice of barriers can impede only the transition rates R_{ij} as in this case $e^{-\beta_b B_{ij}} < 1$. The variance of the barriers is scaled with the system size like that of the energies, so that their ratio is system size independent. Note that numerous other choices of the dynamics for the REM have been studied in the past, most notably, single spin-flip dynamics (see, e.g., Refs. [30–32] and references therein). It would be interesting to search for Mpemba effects in those other choices of REM dynamics as well.

Numerically, we study the parity of the direct Mpemba effect [see Eq. (15)] by exact diagonalization of an ensemble of REM with random barrier R matrices. As an example of typical numerical results, see Fig. 10, where $L = 10$ energy levels are chosen from a Gaussian distribution Eq. (59) and barriers are chosen from Eq. (60). The bath temperature in the numerics is $k_B T_b = 0.1$ and $k_B T_b = 1.0$. Each data point is averaged over 10^5 realizations. From the ample numerical evidence, we infer that the Mpemba effect occurs with finite probability, especially for the $T_b < T_{\text{critical}}$ case (left panel of Fig. 10).

We also study the system size dependence of the REM with random barriers; see Fig. 11. The system size is varied ($L \in [4, 20]$), and we take the bath temperature to be $k_B T_b = 0.1$. The energies are IID from Eq. (59) with variance $\sigma_E^2 \log_2 L$, where $\sigma_E = 1.0$ and the barriers are IID from Eq. (60) with variance $\sigma_B^2 \log_2 L$. Each point on the density plot is averaged over 2×10^5 realizations. We notice that the probability of the parity being positive for the direct Mpemba index seems to be converging to a limiting value with increasing system size. Although we test small sizes, the convergence suggests the thermodynamic limit behavior.

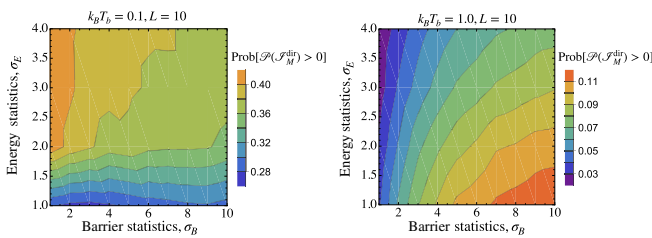


FIG. 10. Lower bound for the probability of the strong Mpemba effect—the probability of the parity being positive for the direct Mpemba index [see Eq. (15)] for the case of REM with random barriers. The number of energy levels is $L = 10$ and the bath temperatures are $k_B T_b = 0.1$ (left) and $k_B T_b = 1.0$ (right). The energies are IID from Eq. (59) with variance $\sigma_E^2 \log_2 L$, and the barriers are IID from Eq. (60) with variance $\sigma_B^2 \log_2 L$. Each point on the density plot is averaged over 10^5 realizations. The condensation phase transition is at $k_B T_{\text{critical}} = \sigma_E / \sqrt{2 \ln 2} \approx 0.84 \sigma_E$. We notice that the probability of having a direct strong Mpemba effect is finite and even high for certain regions of the $\sigma_E \sigma_B$ -plane for $T_b < T_{\text{critical}}$ (left panel).

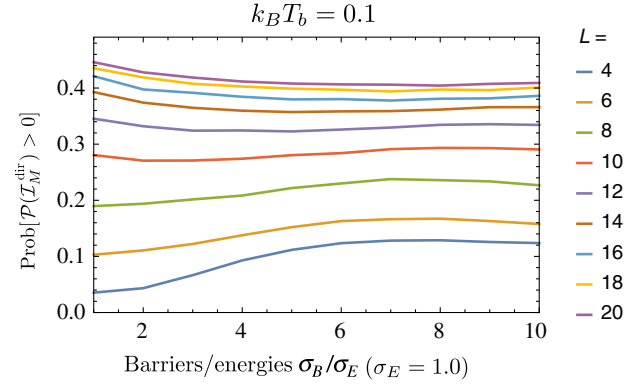


FIG. 11. Lower bound for the probability of the strong Mpemba effect—the probability of the parity being positive for the direct Mpemba index [see Eq. (15)] for the case of the REM with random barriers and different system sizes $L \in [4, 20]$. The bath temperature is $k_B T_b = 0.1$. The energies are IID from Eq. (59) with variance $\sigma_E^2 \log_2 L$ and $\sigma_E = 1.0$, and the barriers are IID from Eq. (60) with variance $\sigma_B^2 \log_2 L$. Each point on the density plot is averaged over 2×10^5 realizations. We notice that the probability of the parity being positive for the direct Mpemba index seems to be converging to a finite limiting value with increasing system size.

VI. DISCUSSION

The Mpemba effect is a shortcut in relaxation time. The direct Mpemba effect implies that initiating the system at a particular hot temperature results in cooling down which is faster than any colder temperature when the system is coupled to a cold bath. Possibly even more counterintuitive is the inverse Mpemba effect where an analog effect happens in heating. Similar to the direct Mpemba effect, in annealing one first heats the system and then cools it in a controlled manner such that it acquires desirable features (relaxes to the ground state, has fewer defects, etc.). More specifically, simulated annealing is a probabilistic technique used to find ground states [33,34], while annealing in metallurgy is used to make materials with larger monocrystal domains and fewer defects [35]. It would be interesting to explore the connection between annealing and the Mpemba effect.

Markov chain Monte Carlo (MCMC) algorithms are essential numerical tools broadly used in many branches of science to estimate steady-state properties of various systems [36]. It is often desirable to speed up the relaxation of a MCMC to the steady state; see, e.g., Refs. [37,38]. Our results serve as proof of principle that in specific systems one could devise additional transition barriers (B_{ij} s) that would cause speed up of a MCMC algorithm's relaxation to equilibrium by creating a strong Mpemba effect.

The approach to equilibrium often has a nontrivial relationship with the energy landscape and nature of the barriers. This is especially true in glassy materials and complex many-body systems. The approach to equilibration can even be used to explore structures in glassy systems and many-body systems experimentally [39]. One of the future

directions is to deepen the understanding of the relation of the Mpemba effect and to the plethora of nontrivial cooling phenomena present in glassy materials such as memory, aging, and rejuvenation.

ACKNOWLEDGMENTS

The work of I. K. is supported by the National Science Foundation Grant No. DMR-1508245. This research is supported in part by the National Science Foundation under Grant No. NSF PHY-1125915. M. V. thanks E. Siggia, G. Falkovich, J. Cohen, and C. Kirst for insightful remarks. O. R. is the incumbent of the Shlomo and Michla Tomarin career development chair, and is supported by a research grant from Mr. and Mrs. Dan Kane and the Abramson Family Center for Young Scientists at WIS. O. R. thanks C. Jarzynski for insightful remarks.

APPENDIX A: HIGH-TEMPERATURE EXPANSION

Here we derive Eq. (51) for the asymptotic T_b^{-1} behavior of the probability of a direct strong Mpemba effect. The starting point is

$$\text{Prob}[\mathcal{P}(\mathcal{I}_M^{\text{dir}}) > 0] = \frac{1}{2} + \frac{1}{\pi} \text{sign}(\mathbf{u}^{\text{dir}} \cdot \mathbf{w}) \arctan \frac{1}{K}, \quad (\text{A1})$$

where K is given in Eq. (42). By plugging Eqs. (38) and (39) into Eq. (42), we get

$$K = \sqrt{\frac{[\sum_{i=1}^L e^{\beta_b E_i} (1 - \frac{L}{Z(T_b)} e^{-\beta_b E_i})^2] \langle \Delta E^2 \rangle_b}{(\sum_{j=1}^L (-E_j + \langle E \rangle_b))^2} - 1}, \quad (\text{A2})$$

where $\langle E \rangle_b \equiv \sum_i \pi_i(T_b) E_i$ and $\langle \Delta E^2 \rangle_b \equiv \sum_i \pi_i(T_b) (E_i - \langle E \rangle_b)^2$. At the high-temperature limit $T_b \rightarrow \infty$, we can expand K in small β_b . To get the correct result, we have to expand all terms in the argument for the square root up to order β_b^2 . Using $\arctan(1/K) \sim (\pi/2) - K$, we find

$$\text{Prob}(-\{a_2(T = \infty)[\partial_T a_2]_{T=T_b}\} > 0) = \frac{C_E}{T_b}, \quad (\text{A3})$$

where

$$C_E = \frac{1}{\pi} |(\bar{E}^2 - \overline{E^2})| (8\bar{E}^6 - 24\bar{E}^4 \overline{E^2} + 20\bar{E}^2 \overline{E^2}^2 - 5\overline{E^2}^3 + 4\bar{E}^3 \overline{E^3} - 2\bar{E} \overline{E^2 E^3} - \overline{E^3}^2 - \bar{E}^2 \overline{E^4} + \overline{E^2 E^4})^{1/2}, \quad (\text{A4})$$

and $\overline{E^k}$ is the k th moment of the energy distribution defined as

$$\overline{E^k} \equiv \frac{1}{L} \sum_{i=1}^L E_i^k. \quad (\text{A5})$$

APPENDIX B: PROOF OF REALIZABILITY OF THE ISOTROPIC ENSEMBLE

Theorem 1.—Given any choice of a real vector \mathbf{f}_2 orthogonal to \mathbf{f}_1 in Eq. (34), there exists a set of barriers B_{ij} with relaxation dynamics obeying detailed balance (4) having $F^{-1/2} \mathbf{f}_2$ as its slowest relaxation eigenvector.

Proof.—For our purpose, we need to demonstrate at least one choice of barriers. We first note that for any (symmetrized) form of the driving \tilde{R} with a steady-state distribution \mathbf{f}_1 , we can obtain, using Eqs. (4) and (8), formally, a set of barriers as

$$B_{ij} = -\frac{1}{\beta_b} \left(\log(\tilde{R}_{ij}) - \frac{E_i + E_j}{2} \right), \quad i \neq j. \quad (\text{B1})$$

The only requirement for these B_{ij} 's to be consistent with our relaxation dynamics is that B_{ij} is a real and symmetric matrix. In other words, it is sufficient that \tilde{R}_{ij} is symmetric and that $\tilde{R}_{ij} > 0$ for all $i \neq j$ (note that R_{ii} is then uniquely determined by the condition that \mathbf{f}_1 is an eigenvector with eigenvalue 0).

We now show that we can make such a choice for any \mathbf{f}_2 . To do so, we consider first an initial set of barriers $B_{ij} = E_i + E_j$. An explicit calculation shows that the resulting dynamics has a single zero eigenvalue associated with \mathbf{f}_1 , and that the rest of the eigenvalues are all $-Z(T_b)$. In this case, we have $\tilde{R}_{ij} = e^{-\{\beta_b(E_i + E_j)\}/2}$. In particular, any choice of \mathbf{f}_2 orthogonal with \mathbf{f}_1 is immediately an eigenvector of \tilde{R} . It remains to break the degeneracy between \mathbf{f}_2 and the other vectors orthogonal to \mathbf{f}_1 . We do this by adding a small perturbation to \tilde{R} :

$$\tilde{R}_{ij} \rightarrow \tilde{R}_{ij} + \frac{\epsilon}{\|\mathbf{f}_2\|^2} (\mathbf{f}_2)_i (\mathbf{f}_2)_j. \quad (\text{B2})$$

This change will affect only the eigenvalue associated with \mathbf{f}_2 , changing it to $-Z(T_b) + \epsilon$, making it a nondegenerate eigenvector.

Clearly, for ϵ small enough the positivity of \tilde{R}_{ij} for $i \neq j$ will not be affected, and the formula (B1) will give us a valid set of barriers. [It is enough to take $\epsilon < \min_{ij} (e^{-\{\beta_b(E_i + E_j)\}/2})$]. *QED.*

Of course, the above procedure yields a very particular type of barrier for each \mathbf{f}_2 . There are numerous ways to set up other barriers consistent with a given \mathbf{f}_2 .

-
- [1] Aristotle, *Meteorologica*, translated by H. D. P. Lee (Harvard University Press, Cambridge, MA, 1962), Book I, Chap. XII, pp. 85–87.
 [2] E. B. Mpemba and D. G. Osborne, *Cool?*, *Phys. Educ.* **4**, 172 (1969).

- [3] S. M. Mirabedin and F. Farhadi, *Numerical Investigation of Solidification of Single Droplets with and without Evaporation Mechanism*, *Int. J. Refrig.* **73**, 219 (2017).
- [4] D. Auerbach, *Supercooling and the Mpemba Effect: When Hot Water Freezes Quicker than Cold*, *Am. J. Phys.* **63**, 882 (1995).
- [5] M. Vynnycky and S. Kimura, *Can Natural Convection Alone Explain the Mpemba Effect?*, *Int. J. Heat Mass Transfer* **80**, 243 (2015).
- [6] X. Zhang, Y. Huang, Z. Ma, Y. Zhou, J. Zhou, W. Zheng, Q. Jiang, and C. Q. Sun, *Hydrogen-Bond Memory and Water-Skin Supersolidity Resolving the Mpemba Paradox*, *Phys. Chem. Chem. Phys.* **16**, 22995 (2014).
- [7] Y. Tao, W. Zou, J. Jia, W. Li, and D. Cremer, *Different Ways of Hydrogen Bonding in Water—Why Does Warm Water Freeze Faster than Cold Water?*, *J. Chem. Theory Comput.* **13**, 55 (2017).
- [8] J. I. Katz, *When Hot Water Freezes Before Cold*, *Am. J. Phys.* **77**, 27 (2009).
- [9] J. D. Brownridge, *When Does Hot Water Freeze Faster than Cold Water? A Search for the Mpemba Effect*, *Am. J. Phys.* **79**, 78 (2011).
- [10] H. C. Burridge and P. F. Linden, *Questioning the Mpemba Effect: Hot Water Does Not Cool More Quickly than Cold*, *Sci. Rep.* **6**, 37665 (2016).
- [11] J. I. Katz, *Reply to Burridge & Linden: Hot Water May Freeze Sooner than Cold*, [arXiv:1701.03219](https://arxiv.org/abs/1701.03219).
- [12] P. Chaddah, S. Dash, K. Kumar, and A. Banerjee, *Overtaking While Approaching Equilibrium*, [arXiv:1011.3598](https://arxiv.org/abs/1011.3598).
- [13] P. A. Greaney, G. Lani, G. Cicero, and J. C. Grossman, *Mpemba-like Behavior in Carbon Nanotube Resonators*, *Metall. Mater. Trans. A* **42**, 3907 (2011).
- [14] A. Lasanta, F. V. Reyes, A. Prados, and A. Santos, *When the Hotter Cools More Quickly: Mpemba Effect in Granular Fluids*, *Phys. Rev. Lett.* **119**, 148001 (2017).
- [15] Y.-H. Ahn, H. Kang, D.-Y. Koh, and H. Lee, *Experimental Verifications of Mpemba-like Behaviors of Clathrate Hydrates*, *Korean J. Chem. Eng.* **33**, 1903 (2016).
- [16] C. Hu, J. Li, S. Huang, H. Li, C. Luo, J. Chen, S. Jiang, and L. An, *Conformation Directed Mpemba Effect on Polylactide Crystallization*, *Cryst. Growth Des.* **18**, 5757 (2018).
- [17] T. Keller, V. Torggler, S. B. Jäger, S. Schütz, H. Ritsch, and G. Morigi, *Quenches across the Self-Organization Transition in Multimode Cavities*, *New J. Phys.* **20**, 025004 (2018).
- [18] Z. Lu and O. Raz, *Nonequilibrium Thermodynamics of the Markovian Mpemba Effect and Its Inverse*, *Proc. Natl. Acad. Sci. U.S.A.* **114**, 5083 (2017).
- [19] N. G. van Kampen, *Stochastic Processes in Physics and Chemistry* (Elsevier, New York, 2001).
- [20] For simplicity, we consider here only ergodic finite-state systems. Much of the analysis can be easily generalized to infinite systems as well.
- [21] D. Mandal and C. Jarzynski, *A Proof by Graphical Construction of the No-Pumping Theorem of Stochastic Pumps*, *J. Stat. Mech.* (2011) P10006.
- [22] For detailed balance matrices R , the eigenvalues are in fact all real. We use this more general notation as our discussion can also be relevant to R 's that do not satisfy the detailed balance.
- [23] The above definition of the Mpemba effect is readily generalizable for the degenerate case, $|\text{Re}\lambda_2| = |\text{Re}\lambda_3|$.
- [24] Since the relaxation described by Eq. (1) reaches the bath's Boltzmann distribution at infinite times, the actual observed relaxation time may depend on the choice of a distance function on the probability simplex. The distance function may be relative entropy or other measures, as long as the exponential ratio between the time-dependent coefficients of v_3 and v_2 is not compensated by the fact that the distances are measured along different directions. In other words, the metric does not grow exponentially faster in one direction compared to the other.
- [25] E. Vives, T. Castán, and A. Planes, *Unified Mean-Field Study of Ferro- and Antiferromagnetic Behavior of the Ising Model with External Field*, *Am. J. Phys.* **65**, 907 (1997).
- [26] R. J. Glauber, *Time Dependent Statistics of the Ising Model*, *J. Math. Phys. (N.Y.)* **4**, 294 (1963).
- [27] L. C. Lapas, R. M. S. Ferreira, J. M. Rubí, and F. A. Oliveira, *Anomalous Law of Cooling*, *J. Chem. Phys.* **142**, 104106 (2015).
- [28] R. Muñoz-Tapia, R. Brito, and J. M. R. Parrondo, *Heating without Heat: Thermodynamics of Passive Energy Filters between Finite Systems*, *Phys. Rev. E* **96**, 030103 (2017).
- [29] B. Derrida, *The Random Energy Model*, *Phys. Rep.* **67**, 29 (1980).
- [30] G. B. Arous, A. Bovier, and V. Gayrard, *Aging in the Random Energy Model*, *Phys. Rev. Lett.* **88**, 087201 (2002).
- [31] G. B. Arous and J. Černý, *Dynamics of Trap Models*, in *Mathematical Statistical Physics*, Les Houches, Vol. 83, edited by A. Bovier, F. Dunlop, A. van Enter, F. den Hollander, and J. Dalibard (Elsevier, New York, 2006), pp. 331–394.
- [32] M. Baity-Jesi, G. Biroli, and C. Cammarota, *Activated Aging Dynamics and Effective Trap Model Description in the Random Energy Model*, *J. Stat. Mech.* (2018) 013301.
- [33] V. Černý, *A Thermodynamic Approach to the Traveling Salesman Problem: An Efficient Simulation*, *J. Optim. Theory Appl.* **45**, 41 (1985).
- [34] S. Kirkpatrick, C. D. Gelatt, and M. P. Vecchi, *Optimization by Simulated Annealing*, *Science* **220**, 671 (1983).
- [35] H. Y. Sohn and S. Sridhar, *1-Descriptions of High-Temperature Metallurgical Processes*, in *Fundamentals of Metallurgy*, Woodhead Publishing Series in Metals and Surface Engineering, edited by S. Seetharaman (Woodhead Publishing, Cambridge, England, 2005), pp. 3–37.
- [36] A. Sokal, *Monte Carlo Methods in Statistical Mechanics: Foundations and New Algorithms*, in *Functional Integration*, NATO ASI Series Vol. 361, edited by C. DeWitt-Morette, P. Cartier, and A. Folacci (Springer, New York, 1997), pp. 131–192.
- [37] K. S. Turitsyn, M. Chertkov, and M. Vucelja, *Irreversible Monte Carlo Algorithms for Efficient Sampling*, *Physica (Amsterdam)* **240D**, 410 (2011).
- [38] M. Vucelja, *Lifting—A Nonreversible Markov Chain Monte Carlo Algorithm*, *Am. J. Phys.* **84**, 958 (2016).
- [39] A. Samarakoon, T. J. Sato, T. Chen, G.-W. Chern, J. Yang, I. Klich, R. Sinclair, H. Zhou, and S.-H. Lee, *Aging, Memory, and Nonhierarchical Energy Landscape of Spin Jam*, *Proc. Natl. Acad. Sci. U.S.A.* **113**, 11806 (2016).